SBR/PVDF based binder for the application of SLMP in graphite anode

Lei Wang,* Yanbao Fu, Vincent S. Battaglia and Gao Liu

A styrene butadiene rubber (SBR) / polyvivylidene difluoride (PVDF) based binder system has been developed for an electrochemical system that is not compatible with the conventional *N*-methyl pyrrolidinone (NMP) solvent used to cast most Li-ion electrode slurries. This polymer system's binding properties decouple the mechanical and ionic-transport properties. It demonstrates comparable mechanical properties as SBR-base electrodes and cell performance as traditional PVDF-based electrodes. This new binder design however enables the incorporation of stabilized lithium metal powder (SLMP) into a graphite anode to improve its first cycle coulombic efficiency.

Lithium ion batteries are the most common rechargeable batteries in consumer electronics.[1] The rapid development of the consumer electronics market has led to a further increase in demand for longer-lasting, higher capacity lithium ion batteries. The state-of-the-art composite electrode design has not changed much since the dawn of the commercialization of the lithium ion battery in the early 1990s.[2] This engineering design of a porous, laminated, composite electrode allows for the high available energy density of the current lithium-ion cell. A primary component of the composite electrode is the polymer binder that ensures that all of the particles remain connected together during hundreds of cycles. The state-of-the-art binder in commercial cells is PVDF, although the use of SBR binder in the anode has gained popularity in recent years.[3,4] Specialty binders such as polyamides,[5] *eg*. LiPAA,[6] have also been reported for lithium ion electrode applications; although, the commercialization of these binders has been limited. The advancement of lithium-ion chemistry in the direction of high energy, high power, and long lifetime has consistently exerted new demands on the overall assembly of the electrode. Therefore, it would not be too surprising that binder materials, although not electrochemically active, need also to advance with the emerging materials.

In commercial lithium-ion batteries, graphite is the most common anode material. Its first cycle coulombic efficiency is *ca*. 90% as a result of the formation of a solid-electrolyte interphase (SEI).[7,8] Furthermore, the capacity of the anode is usually 10% to 15% greater than the capacity of the cathode to prevent lithium deposition. This further negatively impacts the reversible capacity of the full cell. Lithiated graphite combined with stabilized lithium metal powder (SLMP) developed by FMC corporation has been reported to increase the full-cell capacity by 5 to 15%, depending on the irreversible capacity of the preferred graphite material.[9,10] In FMC's proprietary technology, Li metal particles are sealed in a thin coating of Li_2CO_3, which limits the exposure of Li to the ambient environment.[11] SLMP is sprinkled on to a pre-fabricated graphite electrode as a means of incorporating it into a cell and compensating for the irreversible capacity loss. However, the dispersion on to the electrode is difficult to manage during the cell fabrication process, which motivates us to find a better way of incorporating the SLMP into the graphite anode.

As we seek a means for incorporating SLMP into the anode, there are development efforts going on around the world for new binder materials for advanced electrodes,[12,13] unfortunately there are limited detailed reports on the requirements of the binder and the processing conditions, even for the more traditional chemistries. As the most prolific electrode binder, PVDF is dissolved in one of three common solvents, *N*-methyl pyrrolidinone (NMP), dimethyl acetamide (DMA), or dimethyl formamide (DMF). However, SLMP is not compatible with any of these solvents, and can only be dispersed in non-polar solvents, like hexane and toluene. Thus, electrode binders that also dissolve in non-polar solvents need to be considered. This report introduces a new concept of multiple-function binders for electrodes, where mechanical properties and ion transport are equally considered.

The slurry coating process onto the current collector followed by the drying process of the PVDF/NMP based system generates a PVDF network on both the active particles and the conductive additives.[14] As a result, the PVDF binder is situated at the interface between the active material and the electrolyte. The binder not only has to provide mechanical binding among the particles, but also has to allow for ion transport to the active materials from the electrolyte. Therefore, PVDF binders are dual functioning binders that provide mechanical binding and ion transport.[15]

PVDF on its own does not conduct lithium ions; to allow for the transport of ions, PVDF swells with the absorption of electrolyte, by as much as 30% wt.[4] depending on its molecular weight. However, as a result of the swelling, the binding properties diminish significantly. Hence, for PVDF to function as a binder, binder electrolyte swelling and the amount of binder have to be adjusted considered to reach a compromise. In some respects, the cell energy, power, and life can be traced back to the binder.

In an ideal electrode composition, the mechanical binding properties would be decoupled from the ion transport in that the

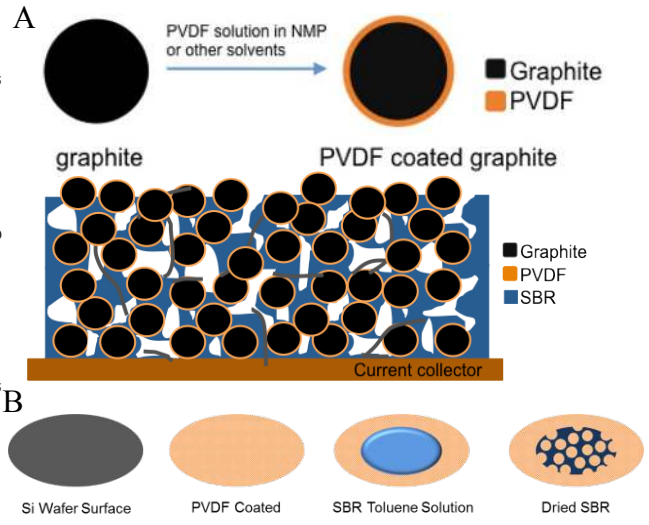

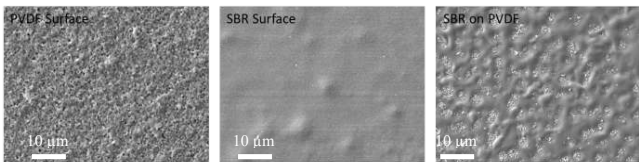

Figure 1. A) Schematic model of PVDF coated graphite laminate. B) Schematic model of the dual coating process and SEM images of PVDF, SBR, and SBR on PVDF.

amount of binder needed for holding the particles together would not affect the rate of ion transport. SBR can be considered in this class, because its mechanical properties can be adjusted by the ratio of the styrene monomer to the butadiene monomer: the higher the styrene content, the higher its rigidity. Furthermore, the swelling of the SBR with electrolyte is small, as the polarity of the SBR stays constant. PVDF binder with its ability to take up electrolyte is a good material for forming ion transport channels at an interface. It is also stable toward lithiated graphite and pliable enough to withstand the limited amount of volume expansion and contraction during cell cycling. The concept of a thin layer of PVDF coated graphite coupled with a small amount of SBR can result in a binder system with both ion transport and mechanical binding capabilities (figure 1A). The challenge in creating such a system stems from the fact that the SBR and PVDF do not readily mix and tend to phase separate when in contact with each other. This is demonstrated by spin coating SBR and PVDF on a Si surface, figure 1B. The image on the left is that of a thin coating of PVDF on Si. The surface appears very rough. The image in the center is that of a thin coating of SBR on Si, where the binder appears smooth. In the image on the right, a thin layer of PVDF was first coated onto a Si surface, followed by a second coating layer of SBR. The SBR layer self-organizes on the PVDF surface to form a porous structure as a result of the poor wetting of SBR on PVDF. This phase-separated structure of SBR and PVDF provides pathways around a top coating of SBR allowing electrolyte to come in contact with the electrode particles when submersed. When 1 to 2% PVDF is coated on the surface of graphite, the graphite particles appear the same under SEM as non-coated graphite but the surface properties are those of PVDF. If such a coating is scrapped off a substrate, ground, and then mixed with a solution of SBR binder, the SBR provides interparticle binding that mechanically stabilizes the electrode without completely covering the graphite particles. The net effect is a long range network of SBR binder that provides robust mechanical stability for the entire electrode, with local ion transport from the electrolyte to the graphite particles through the swollen PVDF undercoating.

The rest of this paper includes a more in-depth description of the electrode fabrication process, some electrode characterization, and some performance results in half cells.

Experiment

Materials.— A CGP-G8 graphite (Conoco Phillips) was used as the anode material. Battery-grade acetylene black (AB) with an average particle size of 40 nm and a material density of 1.95 g/cm^3 was acquired from Denka Singapore Private Limited. PVDF no. 1100 binder with a material density of 1.78 g/cm^3 was supplied by Kureha, Japan. The Stabilized Lithium Metal Powder (SLMP) was supplied by FMC Lithium Corp. SBR and anhydrous NMP were purchased from Aldrich Chemical Company.

Electrolyte uptake.— PVDF and SBR were dissolved in NMP and toluene, respectively. The solutions were magnetically stirred overnight to fully dissolve the binders. Glass O rings were placed onto a Teflon plate. The binder solution was dripped into the O rings, and then the plate was heated to 70°C in an oven to evaporate the solvent. Afterwards, the plate was heated to 130°C for 16 hours in a vacuum oven to remove any moisture. The plate was transferred into a glove box once the oven chamber returned to ambient temperature.

The binder film was carefully stripped off the plate. The mass of film was recorded. Then the film was dipped into a 1M $LiPF_6$ EC/DEC electrolyte for different time intervals. Upon removal from the electrolyte, the film was blotted dry. The mass was not recorded until the reading stabilized.

Binder film imaging.— For the mixture films of PVDF and SBR, a 10% PVDF solution was first spin coated onto a Si surface at the rate of 2000 RPM. This was followed by the spin coating of 5% SBR solution. The dual film was dried in a vacuum oven at 130°C for 16 hours. As a reference, a single layer film of SBR and PVDF were also prepared by spin coating. The surface morphology of the films was imaged by a JEOL JSM-7500F field-emission scanning electron microscope (FESEM).

Electrode casting.— The anode mixture (AB/Binder/CGP-G8) was combined using a Polytron PT10-3S homogenizer at 3000 RPM until a uniform, viscous slurry was acquired. To obtain the best cell performance, the electrode slurry either contained 3% AB/15% PVDF/82% CGP-G8 or 5% AB/5% SBR/90% CGP-G8. The anode laminates for coin-cell testing were cast on 12 µm thick battery-grade Cu sheet using a Mitutoyo doctor blade and a Yoshimitsu Seiki vacuum drawdown coater. The laminates were dried at 130 °C under 10^{-2} Torr vacuum for 16 h. The laminate thickness was measured with a Mitutoyo micrometer with an accuracy of 1 µm. The typical thickness of the AB/Binder/CGP-G8 film was *ca*. 80 µm with an initial porosity of *ca*. 52%. The electrodes were compressed to 35% porosity using a rolling mill with a continuously adjustable gap from International Rolling Mill prior to coin cell assembly.

To prepare a PVDF-coated graphite electrode, 98% CGP-G8 was first mixed with 2% PVDF in NMP to form a slurry. Then a thick layer of slurry was cast on Cu foil and subsequently scraped off after drying. The coated graphite was ground into fine particles in a ball mill, and then mixed with AB and SBR in toluene to form a slurry to cast the final electrode composition. The electrode slurry contained 5% AB/5% SBR/and 90% PVDF-coated CGP-G8 plus toluene.

To prepare a lithium compensated graphite electrode, 2% SLMP was first homogenized with PVDF-coated CGP-G8 and AB in toluene, after which SBR was added. The slurry was mixed again at 4000 rpm for 15 mins. The electrode slurry contained 5% AB/5% SBR/2% SLMP/and 88% PVDF-coated CGP-G8.

Stress-strain measurement— 2 × 4 cm strips were cut out from

the dried electrode laminate. In order to determine the stress-strain curve, the electrode film was peeled off of the Cu current collector. The pulling stress was measured by a Chatillon TCD225 digital force tester with a stretching rate of 2 mm/min.

Coin cell fabrication— Coin cell assembly was prepared in standard 2325 coin cell hardware with CGP-G8 graphite as the active anode material. A 9/16 inch diam disk was punched out from the anode laminate for use in the coin cell assembly. Lithium metal was cut to an 11/16 inch diam disk to serve as the counter electrode. The anode was placed in the center of the outer shell of the coin cell assembly and 50 µl of 1M $LiPF_6$ in EC:DEC (1:1 weight ratio) electrolyte was added to wet the electrode. A 2 cm diam of Celgard 2400 porous polyethylene separator was placed on top of the anode electrode. The counter electrode was placed on top of the separator. Special care was taken to align the counter electrode symmetrically above the anode. A stainless steel spacer and a Belleville spring were placed on top of the counter electrode. A plastic grommet was placed on top of the outer edge of the electrode assembly and crimped closed with a custom-built hydraulic crimping machine manufactured by the National Research Council of Canada. The entire cell fabrication procedure was performed in an argon-filled glove box with an oxygen level below 0.5 ppm and dew point below -80 °C.

Binder Mechanical Properties and Wetting Properties

To assess the mechanical properties of electrode laminates made of different binders and binder combinations, electrode laminates were stretched at a constant rate to their breaking point with a TCD225 digital force tester. Figure 2A shows the pull test results for different laminates with the same dimensions of 4 cm × 2 cm × 80 µm. The electrode laminate can be considered a ductile material, as reflected by the stress-strain curve. For all three electrode laminates, the stress increases with strain initially, and then decreases sharply to a plateau after partial rupture. The electrode laminates tend to break from the sides instead of across the center, resulting in a relatively extended rupture region. The stress drops to zero once the laminate is completely severed. The Young's modulus can be estimated by the slope of the elastic region during the initial stretching period.

$$Young's\ modulus = {}^{stress}/_{strain} = \frac{F/A}{\Delta L/L}$$

where F is the strength stress, A is the section area, ΔL is the increase in length of the electrode, and L is the film length. For the PVDF binder, the stress increases proportionally with the strain until partial rupture at 0.6%. The stress-strain curve of PVDF/SBR overlaps with that of SBR alone, and shows the same Young's modulus, indicating that it is the SBR that provides the binding function. Both the PVDF/SBR and SBR curves increase proportionally and show elastic behaviour initially. In contrast to the PVDF, the PVDF/SBR and SBR curves start to bend over at the yield strain of 2.3%, which can be determined by the offset method with the arbitrary value of 0.2%. The yield point, ultimate point, and Young's modulus for laminates made of SBR, PVDF, and PVDF/SBR are summarized in table I. Of the three binders, SBR has the highest ultimate strength, due to its higher elastic properties which allows for a higher degree of elongation. PVDF/SBR has slightly lower strength than SBR, which is probably due to incomplete de-aggregation of the PVDF covered graphite in the ball mill. The uneven distribution of particle sizes may impair the SBR's coverage. The PVDF electrode laminate has a much lower yield point and much higher Young's modulus, distinguishing itself from the SBR/PVDF and SBR binder systems.[16]

Table I. Mechanical properties for electrode laminates made of different binders.

	SBR	*PVDF*	*PVDF/SBR*
Yield strain	2.3%	0.6%	2.3%
Yield strength	5.6 MPa	3.8 MPa	5.7 MPa
Ultimate strain	7.3%	0.6%	5.0%
Ultimate strength	7.7 MPa	3.8 MPa	7.0 MPa
Young's modulus	359 MPa	645 MPa	392 MPa

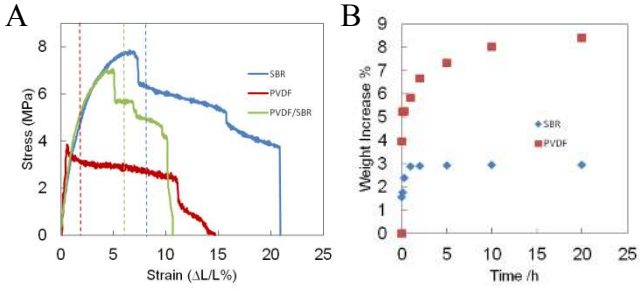

Figure 2. A) Pull test for electrode laminates made of PVDF, SBR and PVDF/SBR. B) Swelling ratio *vs* swelling time in 1M $LiPF_6$ EC/DEC electrolyte for PVDF and SBR.

To compare the swelling properties of the SBR and PVDF, thin films of 100 µm were prepared by drying the binder solution on top of a Teflon surface. The films were then dipped into a 1M $LiPF_6$ EC/DEC electrolyte for different time intervals. Immediately upon removal of the electrodes from the electrolyte, the films were blotted dry and weighed. Figure 2B displays the swelling ratio of the PVDF and SBR *versus* time. Swelling of the binders occurred immediately upon immersion in the electrolyte and took hours to achieve saturation. The weight increase of SBR is 3% after 20 hours. The electrolyte uptake is about 9% for the PVDF film after 20 hours and continues to increase, which is about 3 times that of SBR. As such, when PVDF is used as the binder in an electrode, the large amount of electrolyte uptake by PVDF makes it conducive to ion transport to the graphite. On the other hand, the electrolyte uptake by the PVDF reduces the adhesion strength between particles and between the laminate and current collector. Conversely, SBR only provides mechanical binding between particles and very limited swelling of electrolyte.

Cell Performance

The anodes were assembled in standard 2325 coin cell hardware. A Maccor Battery Test system was used to measure the performance of the coin cells held at 30°C in an environmental chamber. The first cycle coulombic efficiency, reversible capacity, and rate capability of the graphite anodes with different binders were investigated in 1 M $LiPF_6$/EC:DEC (1:1) electrolyte against a Li foil counter electrode. Three formation cycles were conducted at the rate of C/20 between 1.0 and 0.01 V. Capacity of each cell was determined from the last formation cycle and

was used to estimate the C rate for all subsequent cycles. Figure 3A shows the rate performance of the graphite electrodes with PVDF, SBR, and a combination of PVDF and SBR. These electrodes were first lithiated at C/10 and then delithiated at different rates of C/10, C/5, C/2, 1C, 2C, 5C, 10C, and 20C. The cells with PVDF and PVDF/SBR give very similar performance. Cell capacity remains above 300 mAh/g up to a rate of 5C, indicating that the capacity is not terribly affected by Li-ion diffusion at these rates. Cell capacity starts to drop dramatically at the rate of 10C, indicating that 5C is the maximum current for this graphite anode to deliver a majority of its capacity. Conversely, the cell capacity drops steadily with increasing current rate for cells with just SBR binder, indicating a more limiting capacity loss mechanism than cells with PVDF binder. Since SBR is non-wetting of electrolyte, Li ion diffusion resistance in the SBR matrix arises rapidly with discharge rate, and becomes the determining factor controlling the rate of the electrochemical reaction. Alternatively, coating small amounts of PVDF on the graphite surface can improve its performance significantly. As introduced in the model (figure 1), in the absence of PVDF, graphite particles are wrapped up tightly by the insolating SBR network. The coating of PVDF on the graphite is non-wetting by SBR, resulting in patches of uncovered PVDF and thus opening channels in the SBR network for electrolyte to reach the graphite particles. In this way, the mechanical binding of particles is decoupled from the ion transport. The binding strength is as good as that with SBR alone, and the cell performance is as good as that with PVDF alone.

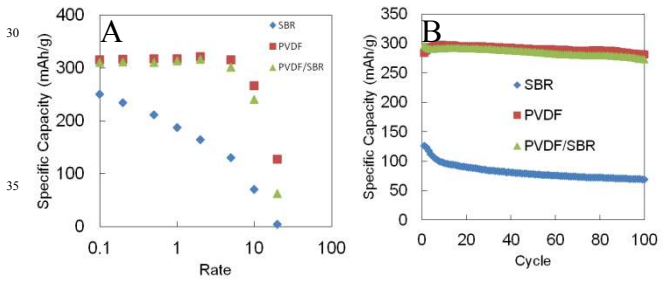

Figure 3. Cell performance of CGPG-8 with different binders: SBR, PVDF and PVDF/SBR. A) Rate performance: cell was lithiated at C/10 and delithiated with different rates. B) Cycling performance: cell was lithiated at C/5 and delithiated at C/2

Cycling performance was conducted at a lithiation rate of C/5 and delithiation rate of C/2; results are provided in figure 3B. The reversible cell capacities for graphite with PVDF and PVDF/SBR binders are ~300 mAh/g. After 100 full capacity cycles, the cells retained more than 90% of their initial capacity. The reversible cell capacity for the graphite with SBR binder is only 1/3 of the capacity of graphite with PVDF binder. Half of the capacity loss happens in the first 10 cycles and is ascribed to the SEI rearrangement at the graphite anode surface.[17,18] High concentrations of binder can accommodate stress build up during the volume change of the graphite, allowing more cycles at higher loading of active materials. Therefore, high performance batteries such as for power tools need to use PVDF to ensure long life and high current. SBR could be a better material because it is more elastic, allowing for a higher degree of elongation to accommodate the volume change of graphite. However, SBR is a non-polar material so it does not swell with typical Li-ion electrolytes. When a high content of SBR is used, although its binding surpasses PVDF, the SBR isolates the active materials from the electrolyte, resulting in rapid capacity loss.

Coulombic Efficiency Improvement by SLMP

SLMP consists of a stabilizing layer of Li_2CO_3 encapsulating Li metal particles. The material consists of at least 95% Li. Figure 4A shows the SEM image of the particles with a distribution of 10 to 50 μm in diameter. To form the lithiated graphite electrode, 2% SLMP was homogenized with PVDF-coated graphite in toluene to form a slurry that was then cast on a current collector as shown schematically in figure 4C. SLMP is stable in toluene, even under intense agitation. In the composite electrode, SLMP, graphite, and AB were distributed uniformly in an SBR 3D network as shown in figure 4B. Because SLMP consists of a layer of carbonate, the electrode was calendered to break the coating and expose the lithium. Upon the addition of electrolyte, the lithium will be oxidized. The scheme is for it to intercalate into graphite to replace lithium lost to SEI formation or react directly with the electrolyte to assist in forming the SEI on the graphite.

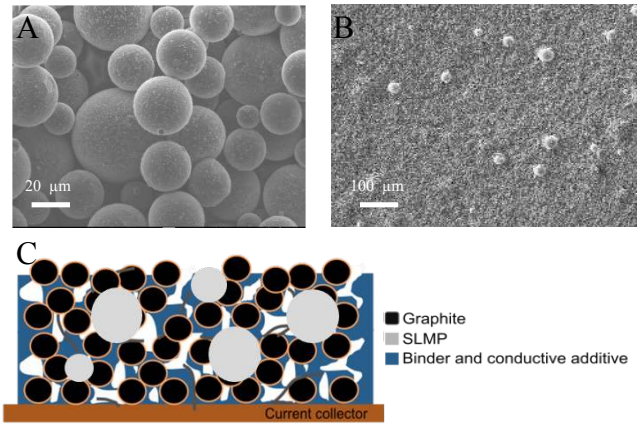

Figure 4. A) SEM image of the SLMP. B) SEM image of the SLMP incorporated graphite anode. C) Schematic model for the SLMP incorporated graphite anode.

Figure 5 compares the first cycle charge/discharge curve for PVDF coated graphite with and without the addition of SLMP. The discharge capacities for both cells are greater than 300 mAh/g. The dash curve for the CGP-G8 graphite-based anode without SMLP is very typical. The open-circuit potential of graphite after assembly in a coin cell is typically 2.1 V. The potential drops with the insertion of Li ions during the charging process. The plateau at 0.6 V is ascribed to the consumption of Li ions during the SEI formation on graphite, resulting in 10% capacity loss in the first cycle. In contrast, the open-circuit potential of the SLMP lithiated graphite starts at 0.2 V, which is below the SEI formation potential of 0.6 V. By controlling the amount of SLMP in the laminate, the capacity lost due to the consumption of lithium during the formation process is compensated for. Hence, the first cycle coulombic efficiency was improved from 90.6% to 96.2%.

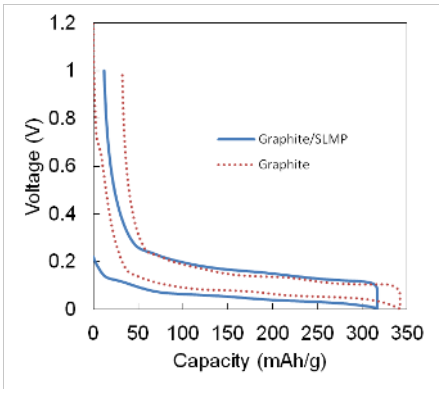

Figure 5. Initial cell formations for the CGP-G8 and CGP-G8/SLMP anodes. Charge/discharge current: C/20

Conclusions

In summary, we introduce the concept of decoupling a binder system's binding properties from its ion transport properties. In the composite graphite electrode, SBR is added to bind the different materials together, while PVDF provides an ion transport function to the surface. The PVDF coated graphite with SBR binder demonstrates comparable mechanical properties as a pure SBR binder electrode and cell performance as a pure PVDF binder electrode. This composite binder system enables the incorporation of SLMP into the graphite anode. The lithium from the SLMP improves the first cycle coulombic efficiency as it contributes to the formation of the SEI. The development of the PVDF/SBR binder system opens a new window for the application of SLMP in other emerging materials, such as hard carbon or Si[19] which display a high capacity but also a significantly high capacity loss in the first cycle.

Acknowledgements

This research was funded by the Assistant Secretary for Energy Efficiency, Office of Vehicle Technologies of the U.S. Department of Energy under contract no. DE-AC03-76SF00098 as part of the Industry-Laboratory Integrated Research Program out of the Office of Vehicle Technologies. FMC-Lithium Inc. is a partner on this project.

Notes and references

Lawrence Berkeley National Laboratory, Environmental Energy Technologies Division, Berkeley, California 94720, USA;
**E-mail: wanglei@lbl.gov*

(1) *Lithium-Ion Batteries: Science and Technologies*; M. Yoshio; R. J. Brodd; Kozawa, A., Eds.; Springer, 2009.

(2) *Lithium Batteries: Science and Technology*; Nazri, G.-A.; Pistoia, G., Eds.; Springer, 2003.

(3) Buqa, H.; Holzapfel, M.; Krumeich, F.; Veit, C.; Novák, P. *J Power Sources* 2006, **161**, 617.

(4) Liu, W.-R.; Yang, M.-H.; Wu, H.-C.; Chiao, S. M.; Wu, N.-L. *Electrochem. Solid-State Lett.* 2005, **8**, A100.

(5) Choi, N.-S.; Yew, K. H.; Choi, W.-U.; Kim, S.-S. *J Power Sources* 2008, **177**, 590.

(6) Magasinski, A.; Zdyrko, B.; Kovalenko, I.; Hertzberg, B.; Burtovyy, R.; Huebner, C. F.; Fuller, T. F.; Luzinov, I.; Yushin, G. *ACS Appl Mater Interfaces* 2010, **2**, 3004.

(7) Chahar, B. S.; Mao, Z. *World Electric Vehicle Journal* **2009**, *3*.

(8) *Lithium-Ion Batteries: Solid-Electrolyte Interphase*; P. B. Balbuena; Wang, Y., Eds.; World Scientific Publishing Company, 2004.

(9) Jarvis, C. R.; Lain, M. J.; Gao, Y.; Yakovleva, M. *J Power Sources* 2005, **146**, 331.

(10) Jarvis, C. R.; Lain, M. J.; Yakovleva, M. V.; Gao, Y. *J Power Sources* 2006, **162**, 800.

(11) Xiang, B.; Wang, L.; Liu, G.; Minor, A. M. *J. Electrochem. Soc.* 2013, **160**, A415.

(12) Xun, S.; Song, X.; Wang, L.; Grass, M. E.; Liu, Z.; Battaglia, V. S.; Liu, G. *J. Electrochem. Soc.* 2011, **158**, A1260.

(13) Ji, L.; Rao, M.; Aloni, S.; Wang, L.; Cairns, E. J.; Zhang, Y. *Energy Environ. Sci.* 2011, **4**, 5053.

(14) Zheng, H.; Zhang, L.; Liu, G.; Song, X.; Battaglia, V. S. *J Power Sources* 2012, **217**, 530.

(15) Tsuchida, E.; Ohno, H.; Tsunemi, K. *Electrochim. Acta* 1983, **28**, 591.

(16) In *IEEE 5th International Symposium on Micro Machine and Human Science proceedings* Nagoya, 1994, p 75.

(17) Dubarry, M.; Liaw, B. Y. *J Power Sources* 2009, **194**, 541.

(18) Vetter, J.; Novák, P.; Wagner, M. R.; Veit, C.; Möller, K. C.; Besenhard, J. O.; Winter, M.; Wohlfahrt-Mehrens, M.; Vogler, C.; Hammouche, A. *J Power Sources* 2005, **147**, 269.

(19) Liu, N.; Hu, L.; McDowell, M. T.; Jackson, A.; Cui, Y. *ACS Nano* 2011, **5**, 6487.